Dyes and Pigments 88 (2011) 109–115

Contents lists available at ScienceDirect

Dyes and Pigments

journal homepage: www.elsevier.com/locate/dyepig

The synthesis, characterization and optical properties of silicon and praseodymium doped Y_6MoO_{12} compounds: Environmentally benign inorganic pigments with high NIR reflectance

Giable George, V.S. Vishnu, M.L.P. Reddy*

Chemical Sciences and Technology Division, National Institute for Interdisciplinary Science and Technology (NIIST), CSIR, Thiruvananthapuram 695 019, Kerala, India

ARTICLE INFO

Article history:
Received 13 May 2010
Accepted 21 May 2010
Available online 1 June 2010

Keywords:
Rare earth molybdates
Near-infrared reflectance
Environmentally benign
Inorganic pigments
Roofing material
'Cool pigments'

ABSTRACT

Novel, yellow, brown and brick-red colored, near-infrared reflective pigments based on yttrium molybdate doped with metal ions such as Si^{4+} or Pr^{4+} are described. Replacing Si^{4+} for Y^{3+} in Y_6MoO_{12} changed the color from light-yellow to dark-yellow and the band gap decreased from 2.60 to 2.45 eV due to O_{2p}-Mo_{4d} charge transfer transitions. In contrast, replacing Pr^{4+} for Y^{3+} changed the color from light-yellow to dark brown and the band gap shifted from 2.60 to 1.90 eV. The coloring mechanism is based on the introduction of an additional $4f^1$ electron energy level of Pr^{4+} between the valence and conduction bands. The NIR reflectance of the pigments on asbestos cement sheet was measured.

1. Introduction

Much interest has attended roofing materials with high solar reflectance and high thermal emittance, so that interiors stay cool, thereby reducing the demand for air-conditioned buildings [1–4]. Solar radiation consists of ~5% UV radiation, 43% visible radiation and 52% near-infrared radiation (NIR; ~780–2500 nm). The heat producing region of the infrared radiations ranges from 700 to 1100 nm. Coatings colored with conventional pigments tend to absorb NIR radiation that bears >50% of the power in sunlight resulting in heat build-up [5]. Replacing conventional pigments with "cool pigments" that absorb less NIR radiation can provide coatings similar in color to that of conventional roofing materials, but with higher solar reflectance. NIR reflective pigments have been used in the military, construction, plastics and ink industries [6]. IR reflective screens useful in green houses, made using a polymer and reflective pigments, allow only visible light transmission but reflect NIR light. NIR reflective pigments can also be useful for camouflage applications [7].

Inorganic NIR pigments are mainly metal oxides and are primarily employed in two major applications namely visual camouflage and reduced heat build-up applications. Most of the literature on NIR reflective pigments exists as patents [8–11], which indicate their vast potential application. Complex inorganic pigments based on mixed metal oxides (e.g., chromium green, cobalt blue, cadmium stannate, lead chromate, cadmium yellow and chrome titanate yellow), which have been used in camouflage, absorb visible light but reflect the NIR portion of incident radiation [1,2,5]. However, many of these pigments are toxic and there is a need to develop novel colored, NIR-reflecting inorganic pigments that are less hazardous to the environment. Recently, the industrial utilization of lanthanides has increased rapidly because of their low toxicity; consequently, a large number of rare earth based NIR reflective pigments have been proposed as alternatives to traditional pigments [8,10,12]. In this work, a series of NIR reflective coloured pigments of formula $Y_{6-x}M_xMoO_{12+\delta}$ (where M = Si^{4+} or Pr^{4+} and x ranges from 0 to 1.0) were synthesized and applied to asbestos cement roofing material so as to evaluate their use as 'cool pigments'.

2. Experimental

2.1. Materials and methodology

Stoichiometric powder mixtures of Pr_6O_{11} (99.9%), Y_2O_3 (99.9%), SiO_2 (99.9%) and MoO_3 (99.9%), obtained form Sigma Aldrich, were transferred to an agate mortar and homogenized by wet milling in acetone. Residual acetone was removed by evaporation and the

* Corresponding author. Tel.: +91 471 2515360; fax: +91 471 2491712.
E-mail address: mlpreddy55@gmail.com (M.L.P. Reddy).

0143-7208/$ – see front matter © 2010 Elsevier Ltd. All rights reserved.
doi:10.1016/j.dyepig.2010.05.010

resultant powders were calcined in platinum crucibles in a Nabertherm electric furnace at 1600 °C for 12 h in air. The heating of the furnace was programmed to increase the temperature at 5 °C/min. The ensuing pigment powders were ground in an agate mortar.

A small strip of asbestos cement sheet (made up with small amounts of asbestos fibre locked in cement slurry) was pre-coated with an inexpensive white pigment that is highly reflective to NIR light. $Y_5SiMoO_{12+\delta}$ and $Y_{5.4}Pr_{0.6}MoO_{12+\delta}$ samples were ground, sieved (<35 μm) and ultrasonicated (Vibronics, 250 W, India) for 10 min to ensure complete dispersion of the pigment particles in an acrylic-acralyn emulsion. The pigment:binder ratio was maintained as 1:1 by mass. The viscous pigment solution was applied to the asbestos cement sheet surface and dried.

2.2. Characterization techniques

The phase purity of the calcined pigment samples were determined using powder X-ray diffraction in a diffractometer (Philips X'pert Pro) employing Ni-filtered Cu Kα ($\lambda = 0.154060$ nm) radiation. Data were collected by step scanning over a 2θ range from 20° to 70° with a step size of 0.08° and 5s counting time at each step. The diffuse reflectance of the powdered pigment samples were measured (380–780 nm) using a UV–vis Spectrometer (Shimadzu UV-2450 with an integrating sphere attachment, ISR-2200) using illuminant D_{65}, 10° standard observer and measuring geometry d/8°. For each colorimetric parameter of a sample, measurements were made in triplicate and an average value was chosen as the result. Typically, for a given sample, the standard deviation of the measured colorimetric parameters was <0.10 and the relative standard deviation was ≤1%, indicating that the measurement error can be ignored. The near-infrared reflectance (780–2000 nm) of the powdered pigment samples as well as the pigment coated asbestos cement sheet was measured using a UV–vis–NIR spectrophotometer (Shimadzu, UV–3600 with an integrating sphere attachment, ISR–3100). The diffuse reflectance measurement procedure in both UV–vis and NIR regions used was as follows: a set of powder sample holders filled with Barium sulphate for the visible region and poly–tetrafluoroethylene for the NIR region, was mounted on both the sample and reference sides of the exit port of the integrated sphere to set the baseline measurement. The sample holder was then filled with powder pigment and its reflectance measured; in the case of pigment coated asbestos cement sheet, the coated samples were placed in the sample side of the exit port of the integrating sphere by replacing the standard powder sample holder and their reflectance was measured.

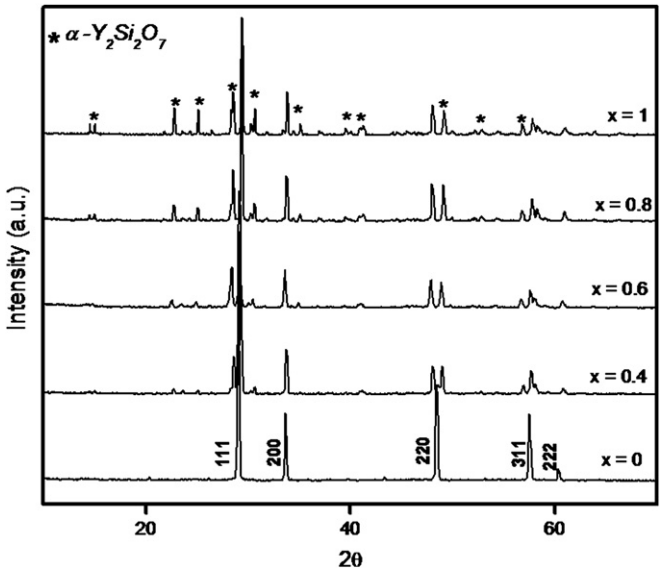

Fig. 1. XRD patterns of $Y_{6-x}Si_xMoO_{12+\delta}$ (*x* ranges from 0 to 1).

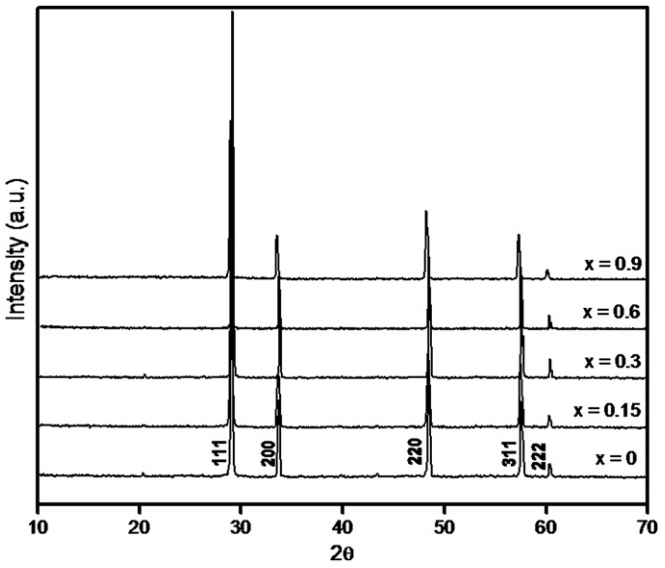

Fig. 2. XRD patterns of $Y_{6-x}Pr_xMoO_{12+\delta}$ (*x* ranges from 0 to 0.9).

Scanning electron micrographs of the samples were taken on a scanning electron microscope (SEM) JEOL JSM–6390 model, with an acceleration voltage of 20 kV. Thermo gravimetric (TG) and differential thermal analyses (DTA) were performed in a Pyris Diamond TG/DTA Perkin Elmer make. All the experiments were run in a platinum crucible from 50 to 1000 °C with a heating rate of 20 °C/min in nitrogen atmosphere and with a sample weight of 8.87 mg. The particle size distribution of the typical pigment sample was investigated in water medium with calgon as the dispersing agent using the laser scattering particle size distribution analyzer (CILAS 930 Liquid). The samples were ultrasonically homogenized for 180 s during measurement and the signal was evaluated on the basis of Fraunhofer bending. The thickness of the pigment coating on asbestos cement sheet was measured employing LEICA DMRX optical microscope.

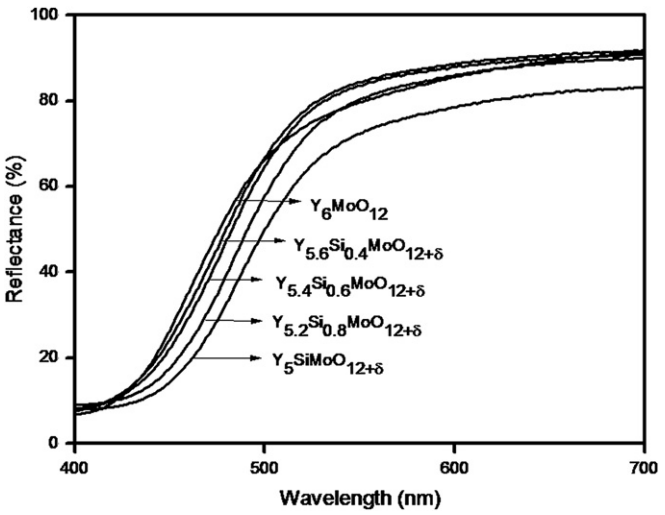

Fig. 3. UV–vis reflectance spectra of powdered $Y_{6-x}Si_xMoO_{12+\delta}$ (*x* ranges from 0 to 1) pigments.

Fig. 4. Photographs of $Y_{6-x}Si_xMoO_{12+\delta}$ and $Y_{6-x}Pr_xMoO_{12+\delta}$ pigments.

3. Results and discussion

3.1. Powder X-ray diffraction analysis

Fig. 1 shows the XRD patterns of $Y_{6-x}Si_xMoO_{12+\delta}$ (x ranges from 0 to 1.0) with different dopant amounts of silicon. The diffraction pattern of Y_6MoO_{12} can be very well indexed to a cubic structure (JCPDF 30–1456) with a lattice constant of 0.5299 nm. The crystal lattice would be distorted with the substitution of Si^{4+} for Y^{3+} in Y_6MoO_{12}. This is due to the smaller ionic radius of Si^{4+} (0.0260 nm) when compared to that of Y^{3+} (0.1019 nm) [13]. Further it can be noted from the XRD patterns that the doping of Si^{4+} for Y^{3+} in Y_6MoO_{12} results in the formation of an additional phase of α-$Y_2Si_2O_7$ (JCPDF 21–1457). On the other hand, the doping of Pr^{4+} (0.096 nm) for Y^{3+} in Y_6MoO_{12} did not alter the phase significantly as can be noted from the XRD patterns given in Fig. 2. The cell parameter value for composition up to 4.3 mol % of Pr^{4+} match very well with the high temperature cubic form of Y_6MoO_{12}, which implies that the cubic form can be stabilized at room temperature by doping with Pr^{4+} of up to 4.3 mol%. Above 4.3 mol%, the lattice constant increases slightly with increase in Pr^{4+} concentration and reaches 0.5332 nm at 12.8 mol%. This increase of lattice constant is resulted from the contribution of substitution of Pr^{4+} for Y^{3+} and introduction of extrinsic vacancies by praseodymium doping, which will expand the lattice [14,15].

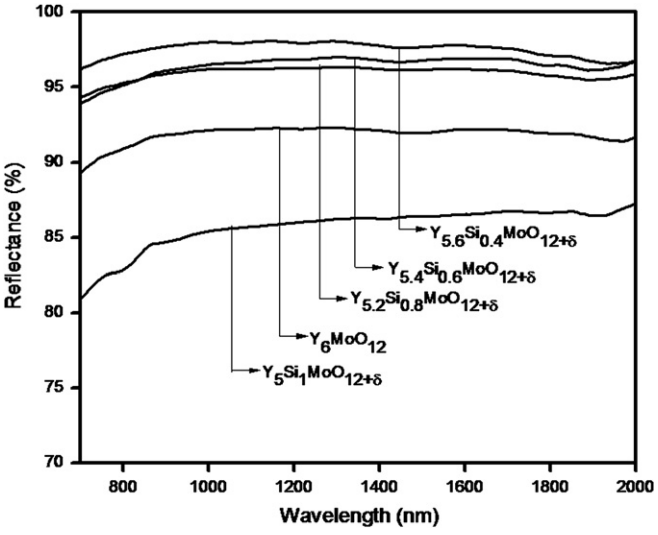

Fig. 5. NIR reflectance spectra of powdered $Y_{6-x}Si_xMoO_{12+\delta}$ pigments.

3.2. Particle size and morphological analysis

Particle size analysis of the typical pigments Y_6MoO_{12}, $Y_5SiMoO_{12+\delta}$ and $Y_{5.4}Pr_{0.6}MoO_{12+\delta}$ reveal a mean diameter of 3.44 μm (size of 90% particles < 6.40 μm, 50% particles < 3.37 μm and 10% particles < 0.14 μm), 8.82 μm (size of 90% particles <20.91 μm, 50% particles < 6.69 μm and 10% particles < 1.31 μm) and 4.61 μm (size of 90% particles < 8.50 μm, 50% particles < 4.32 μm and 10% particles < 0.96 μm), respectively. The homogeneous nature of the pigments can be understood from the SEM images, the average grain size being less than 10 μm, which is again in good agreement with our particle size analysis.

3.3. Effect of silicon doping on the optical properties of Y_6MoO_{12} pigments

The UV–vis diffuse reflectance spectra of the $Y_{6-x}Si_xMoO_{12+\delta}$ (x ranges from 0 to 1) pigment samples are shown in Fig. 3. A strong absorption noted below 485 nm in the UV–vis reflectance spectrum of silicon free Y_6MoO_{12} sample is due to the O_{2p}–Mo_{4d} charge–transfer transition of Mo^{6+} [16–18]. This absorption in the blue region is responsible for the yellow hue of Y_6MoO_{12}, since blue is a complimentary color to yellow. The band gap of the Y_6MoO_{12} pigment is found to be 2.60 eV, which has been obtained by

Table 1
The color coordinates (±0.1) of the $Y_{6-x}Si_xMoO_{12+\delta}$ (x ranges from 0 to 1) powder pigments and band gap values.

Pigment composition	Color coordinates					Band gap (eV)
	L^*	a^*	b^*	C^*	h^o	
Y_6MoO_{12}	89.9	−6.3	48.2	48.6	97.5	2.60
$Y_{5.6}Si_{0.4}MoO_{12+\delta}$	92.9	−7.3	54.3	54.8	97.7	2.54
$Y_{5.4}Si_{0.6}MoO_{12+\delta}$	91.3	−6.9	55.7	56.1	97.1	2.52
$Y_{5.2}Si_{0.8}MoO_{12+\delta}$	89.2	−4.8	60.2	60.3	94.6	2.47
$Y_5SiMoO_{12+\delta}$	87.3	−3.5	62.5	62.6	93.2	2.45

$C^* = [(a^*)^2 + (b^*)^2]^{1/2}$; $h^o = \tan^{-1}(b^*/a^*)$.

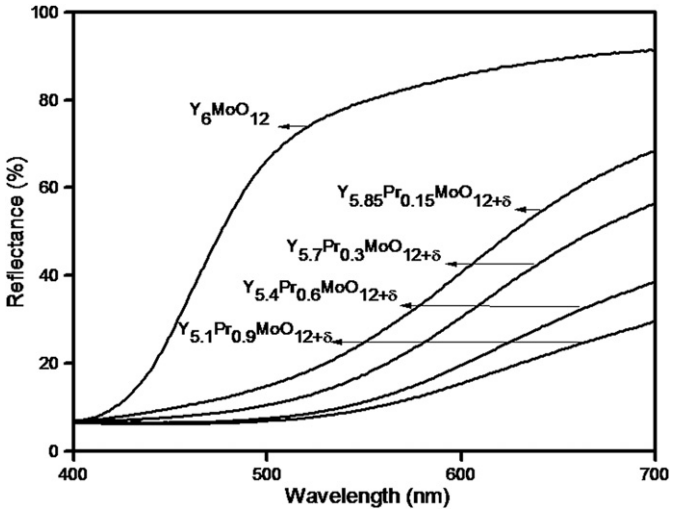

Fig. 6. UV–vis reflectance spectra of powdered $Y_{6-x}Pr_xMoO_{12+\delta}$ (x ranges from 0 to 0.9) pigments.

a straight forward extrapolation method from the corresponding absorption spectrum [19]. It is evident from the reflectance spectra of these pigments that the progressive doping of Si^{4+} for Y^{3+} in Y_6MoO_{12} gently changes the absorption edge from 484 to 510 nm. The introduction of Si^{4+} into the Y_6MoO_{12} lattice results in the formation of an additional phase of α–$Y_2Si_2O_7$ which tends to increase the apparent concentration of Mo^{6+} ions in the lattice. This result in a red shift of the charge transfer band and intensify the yellow hue of Y_6MoO_{12} pigments (Fig. 4). Thus the band gap of the Si^{4+} free pigment sample decreases from 2.60 eV to 2.45 eV, with the increase of silicon concentration (from 5.7 to 14.3 mol%). However, one can conclude that the increase of yellow hue of the pigment sample is really not due to the formation of the impurity phase of α–$Y_2Si_2O_7$.

Fig. 5 depicts the NIR reflectance of the $Y_{6-x}Si_xMoO_{12+\delta}$ (x ranges from 0 to 1) pigment samples. The silicon free sample, Y_6MoO_{12} exhibits 92% NIR reflectance at 1100 nm region. Doping of 5.7 mol% Si^{4+} for Y^{3+} in Y_6MoO_{12} increases the NIR reflectance to 98%. On the other hand, further doping of more and more Si^{4+} for Y^{3+} decreases the NIR reflectance to 86%. The high reflectance in the NIR region exhibited by the designed new class of yellow pigments indicates that these pigment formulations can serve as cool pigments.

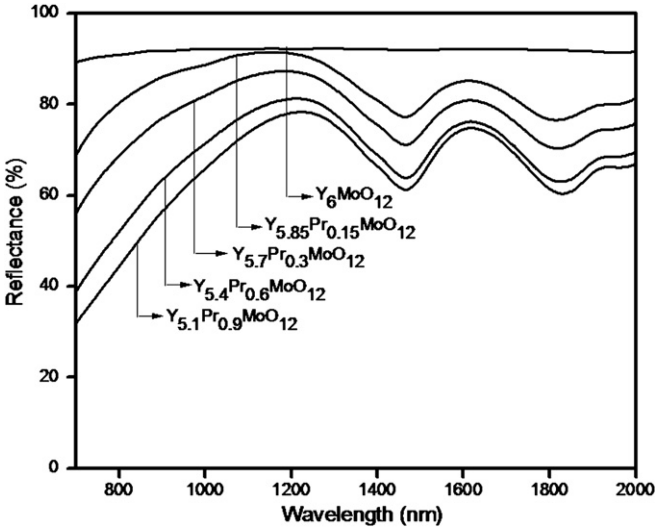

Fig. 7. NIR reflectance spectra of powdered $Y_{6-x}Pr_xMoO_{12+\delta}$ pigments.

Table 2
The color coordinates (±0.1) of the $Y_{6-x}Pr_xMoO_{12+\delta}$ (x ranges from 0 to 0.9) powder pigments and band gap values.

Pigment composition	Color co ordinates					Band gap (eV)
	L^*	a^*	b^*	C^*	h^o	
Y_6MoO_{12}	89.8	−6.3	48.2	48.6	97.5	2.60
$Y_{5.85}Pr_{0.15}MoO_{12+\delta}$	59.5	19.7	36.6	47.0	61.7	1.99
$Y_{5.7}Pr_{0.3}MoO_{12+\delta}$	51.9	20.9	30.9	41.6	55.9	1.95
$Y_{5.4}Pr_{0.6}MoO_{12+\delta}$	42.9	18.7	20.6	37.3	47.7	1.92
$Y_{5.1}Pr_{0.9}MoO_{12+\delta}$	39.3	15.2	15.7	21.9	46.0	1.90

The CIE 1976 color coordinates of the powdered $Y_{6-x}Si_xMoO_{12+\delta}$ (x ranges from 0 to 1) pigment samples are shown in Table 1. The systematic doping of Si^{4+} (from 5.7 to 14.3 mol%) for Y^{3+} in Y_6MoO_{12} results in an increase in the b^* value from 48.2 to 62.5, which shows that yellowness of the pigment samples enhances. At the same time, the increase of Si^{4+} substitution leads to the loss of green hue of the pigment that is evident from the lower values of the color coordinate $-a^*$ (a^* changes from −6.3 to −3.5). The presence of silicon cations in the matrix of Y_6MoO_{12} causes an increase in b^* and decreases the $-a^*$ color coordinate values. Hence the color hue expressed by the color coordinate h° decrease from 97.5 to 93.2. The observed hue angle of the designed pigments are found to be in the yellow region of the cylindrical color space ($h^\circ = 70–105$ for yellow) [20]. Thus the pigments possess yellow hue that are characterized by the improved richness of the yellow color as can be noted from the increase in C^* values (from 48.6 to 62.6). The coloring mechanism of the present pigments is essentially based on the O_{2p}–Mo_{4d} charge transfer transition which further intensify upon doping of Si^{4+} for Y^{3+} in Y_6MoO_{12}.

3.4. Effect of praseodymium doping on the optical properties of Y_6MoO_{12} pigments

Fig. 6 displays the UV–vis diffuse reflectance spectra of the $Y_{6-x}Pr_xMoO_{12+\delta}$ (x ranges from 0 to 1) powdered pigment samples. The doping of 2.1 mol % Pr^{4+} for Y^{3+} in the host lattice of Y_6MoO_{12} introduces an additional energy level due to the $4f^1$ electrons between the O^{2-} valence and Mo^{6+} conduction bands. As a result,

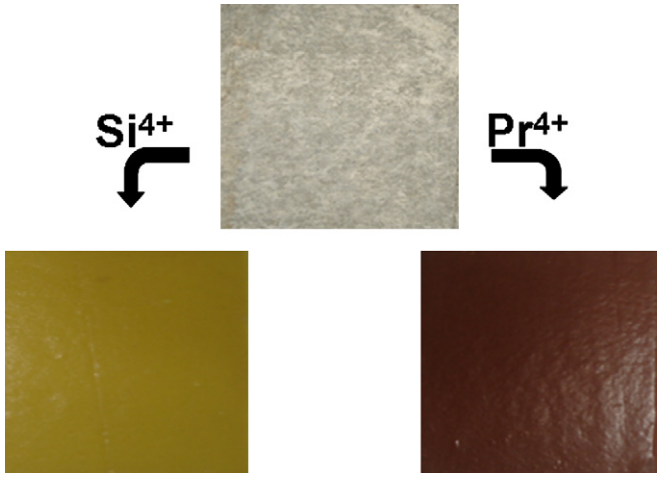

Fig. 8. Photographs of $Y_5SiMoO_{12+\delta}$) and $Y_{5.4}Pr_{0.6}MoO_{12+\delta}$ pigments coated on asbestos cement sheet.

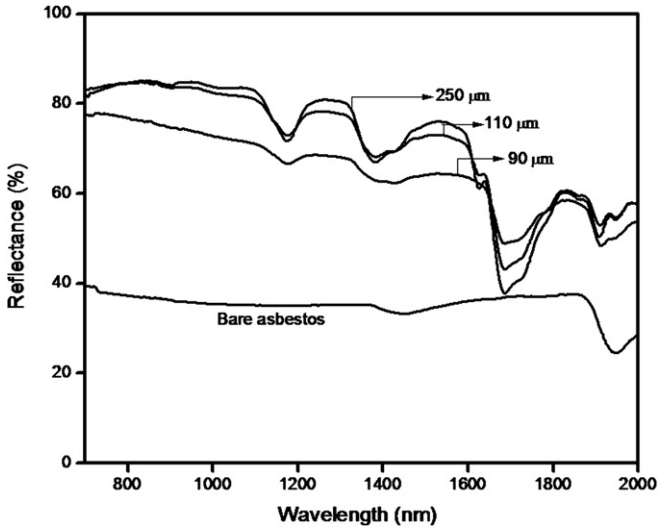

Fig. 9. NIR reflectance spectra of $Y_5SiMoO_{12+\delta}$ pigment coated on asbestos cement sheet with different thickness.

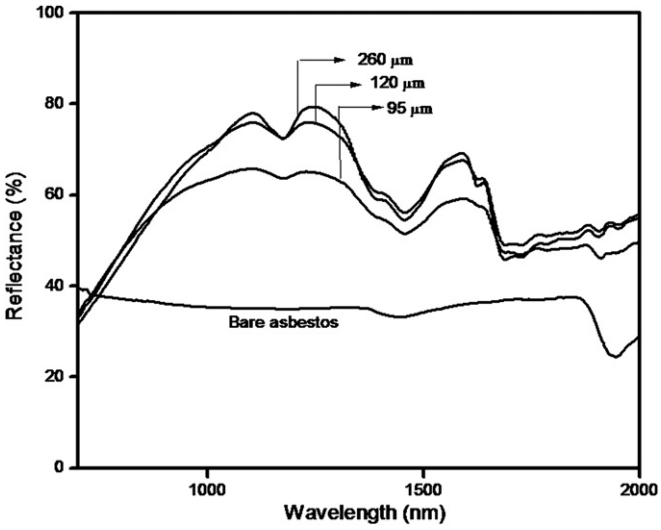

Fig. 10. NIR reflectance spectra of $Y_{5.4}Pr_{0.6}MoO_{12+\delta}$ pigment coated on asbestos cement sheet with different thickness.

the absorption edge is red shifted significantly (from 484 nm to 624 nm) and the band gap of the pigment decreases from 2.60 to 1.99 eV. Therefore, the color of the pigment changes from yellow to brick-red. Further, the more and more substitution of Pr^{4+} (from 4.3 to 12.9 mol%) for Y^{3+} in the host lattice gently red shifts the absorption edge and changes the band gap from 1.99 to 1.90 eV. Consequently the pigment samples changes the color from brick-red to dark brown (Fig. 4).

It can be seen from the NIR reflectance (700–2000 nm) of the praseodymium doped Y_6MoO_{12} powdered pigment samples shown in Fig. 7 that the NIR reflectance decreases (from 92 to 74%) with the increase in concentration of Pr^{4+} from 2.1 to 12.9 mol%. However the high NIR reflectance values clearly highlight the potential for the utility of these pigment samples as cool pigments. The NIR reflectance of the typical powdered brick-red pigment sample, $Y_{5.85}Pr_{0.15}MoO_{12+\delta}$ is found to be higher (88% at 1100 nm) than that of $Ce_{25}Pr_{0.8}FeO_y$ red and $Ce_{25}Pr_{0.8}MoO_y$ orange-red pigments reported elsewhere (<70% at 1100 nm) [12].

From the color coordinates of the Pr^{4+} doped Y_6MoO_{12} powdered pigment samples depicted in Table 2, it is clear that the progressive doping of Pr^{4+} (from 2.1 mol% to 12.9 mol%) for Y^{3+} in Y_6MoO_{12} dramatically decreases the b^* from 48.2 to 15.7. This can be clearly seen from the loss of the yellow hue of the pigment samples with doping of higher concentration of Pr^{4+}. The extent of redness that is expressed by the higher value of color coordinate a^* (from − 6.3 to 20.9) increases up to the content of praseodymium 4.3 mol% ($x = 0.3$). As a result the color changes drastically from yellow to brick–red. Further more and more doping of Pr^{4+} for Y^{3+} (upto 12.9 mol%) decreases the color coordinate a^* value from 20.9 to 15.2. Thus the color of the pigment gently changes from brick–red to dark brown. The pigments have brown hue that are characterized by the lesser richness of color represented by the chroma (C^*) values. The progressive substitution of Pr^{4+} for Y^{3+} in Y_6MoO_{12} significantly decreases the hue angle (h°) from 97.5 to 46.0. The hue angle values reveal that the Pr^{4+} doped pigments lie in the brick red to dark brown region of the cylindrical color space ($h^\circ = 0$–35 for red and 35–70 for orange) [20]. The preceeding trends in color coordinate values could be due to the introduction of a $4f^1$ energy level of praseodymium between the O^{2-} valence and Mo^{6+} conduction bands with the systematic doping of Pr^{4+} ions for yttrium in Y_6MoO_{12}.

3.5. NIR reflectance of the pigments coated on a roofing material (asbestos)

Recently there has been a lot of interest in building roofing materials (like concrete tile, metal, clay tiles, wood and asbestos cement sheets) with high solar reflectance and high thermal emittance such that the interiors stay cool in the sun, reducing demand for cooling power in conditioned buildings and increasing occupant comfort in unconditioned buildings [4,21–23]The reflectance in the near-infrared (NIR) spectrum (700–2500 nm) can be maximized by coloring the top coat with inorganic pigments that weakly absorb and strongly backscatter (optional) NIR radiation. Multiple layers of coatings can be applied to increase reflectance; however, each additional coating increases cost. A two-step, two-layer process has proven more cost-effective. In the present study, the pigment which exhibits best chromatic properties has been chosen to coat on the asbestos cement roofing sheet. The photograph of the coated asbestos cement sheet is given in Fig. 8. The NIR reflectance spectrum of the $Y_5SiMoO_{12+\delta}$ and $Y_{5.4}Pr_{0.6}MoO_{12+\delta}$ samples coated with varying thickness over a base coat of TiO_2 on asbestos cement sheet

Table 3
Effect of coating on the color coordinates (±0.1) of the (a) $Y_5SiMoO_{12+\delta}$ and (b) $Y_{5.4}Pr_{0.6}MoO_{12+\delta}$ coated pigments with different thickness and NIR reflectance (%) values at 1100 nm.

$Y_5SiMoO_{12+\delta}$					$Y_{5.4}Pr_{0.6}MoO_{12+\delta}$				
Thickness (μm)	L^*	a^*	b^*	N (%) 1100 nm	Thickness (μm)	L^*	a^*	b^*	N (%) 1100 nm
90	84.4	−6.6	49.4	71.1	95	47.0	17.9	19.9	65.8
110	84.4	−6.6	49.3	80.9	120	39.7	15.8	16.3	75.6
250	84.6	−4.9	54.6	82.8	260	38.8	15.7	16.2	78.0

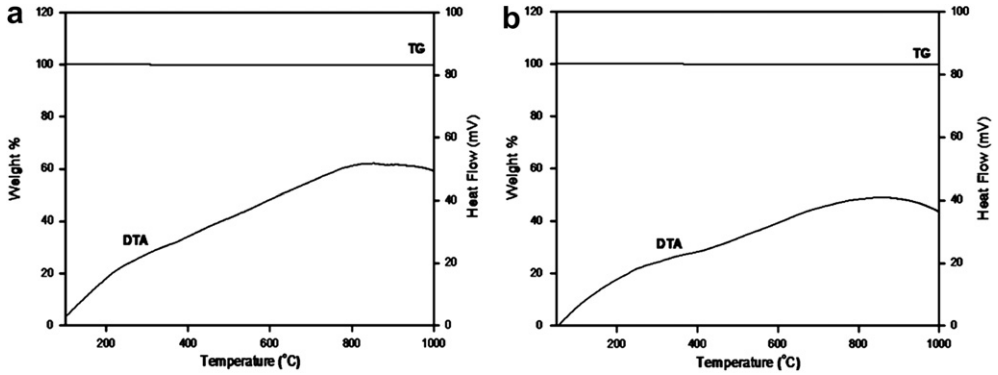

Fig. 11. The TG-DTA of powdered (a) $Y_5SiMoO_{12+\delta}$ and (b) $Y_{5.4}Pr_{0.6}MoO_{12+\delta}$ pigments.

is shown in Figs. 9 and 10, respectively. It is evident from the diffuse reflectance spectrum that the NIR reflectance of the bare asbestos cement roofing sheet shows a low NIR reflectance of 35% (at 1100 nm). The coating of the present pigments has greatly enhanced the NIR reflectance of the asbestos cement sheet. Further it can also be noted that the NIR reflectance increases with increase in thickness of the coatings of the respective pigments (NIR reflectance 71% at 90 μm and 83% at 250 μm for yellow sample; NIR reflectance 66% at 95 μm and 78% at 260 μm for red sample). The data on the color coordinates and NIR reflectance at different thickness of coatings on the asbestos cement roofing material is given in Table 3. As can be noted from the color coordinate data that the b^* value increases (from 49.3 to 54.6) when the thickness of the yellow pigment coating has been almost doubled (110–250 μm). However the $-a^*$ values which represents the green component of the pigment decreases (from −6.6 to −4.9) with increasing thickness from 110 to 250 μm. On the other hand, in the case of the red pigment coating the variation of thickness from 120 to 260 μm does not have much influence on the color coordinates.

3.6. Thermal and chemical stability studies of the pigments

The typical synthesized pigments, $Y_5SiMoO_{12+\delta}$, and $Y_{5.4}Pr_{0.6}MoO_{12+\delta}$, were examined for their thermal stability from 50 to 1000 °C and the results clearly indicate that there is negligible weight loss and phase transition of the pigments (Fig. 11). The acid/alkali and water resistance of the typical pigments $Y_{5.4}Si_{0.6}MoO_{12+\delta}$, and $Y_{5.4}Pr_{0.6}MoO_{12+\delta}$, was investigated with 10% $HCl/H_2SO_4/HNO_3$/NaOH and H_2O. A pre-weighed amount of the pigment was treated with acid/alkali and soaked for half an hour with constant stirring using a magnetic stirrer. The pigment powder was then filtered, washed with water, dried and weighed. Negligible weight loss of pigment was noticed for all the acids, alkali and water tested. The color coordinates of the pigments were measured after acid/alkali and water treatment and the total color difference, ΔE^* of the pigments are found to be negligible as evident from the data reported in Table 4. The above studies highlight that the pigments are chemically and thermally stable.

Table 4
The color coordinates (±0.1) of the (a) $Y_{5.4}Si_{0.6}MoO_{12+\delta}$ and (b) $Y_{5.4}Pr_{0.6}MoO_{12+\delta}$ powder pigments after chemical resistance tests.

$Y_{5.4}Si_{0.6}MoO_{12+\delta}$					$Y_{5.4}Pr_{0.6}MoO_{12+\delta}$			
10% Acid/Alkali	L^*	a^*	b^*	[a]ΔE^*	L^*	a^*	b^*	ΔE^*
H_2O	90.7	−6.8	54.7	0.7	41.9	17.9	19.5	0.8
NaOH	90.2	−6.9	54.1	1.5	41.0	17.6	19.7	1.5
HNO_3	90.3	−6.8	54.6	1.1	41.1	17.9	19.8	1.4
H_2SO_4	90.6	−6.9	54.8	0.8	41.9	17.8	20.9	1.1

[a] $\Delta E^* = [(\Delta L^*)^2 + (\Delta a^*)^2 + (\Delta b^*)^2]^{1/2}$

4. Conclusions

A series of NIR reflective inorganic pigments of formula $Y_{6-x}M_xMoO_{12+\delta}$ (where M = Si^{4+} or Pr^{4+} and x ranges from 0 to 1.0), displayed a wide range of colors from light-yellow to dark-yellow and brick-red to dark brown. The absorption edge of the pigment samples shifted to higher wavelengths (485–510 nm) upon replacing Si^{4+} for Y^{3+} in Y_6MoO_{12}. In contrast, the absorption edge was changed from 485 to 654 nm in the presence of Pr^{4+}. Thus it is evident that various colors can be achieved by the incorporation of suitable metal ions in the Y_6MoO_{12} lattice by tuning of the band gaps. Most importantly, the pigments exhibited high NIR reflectance (75–85%) when coated on asbestos cement sheet, thus rendering them excellent candidates for use as 'Cool Pigments'.

Acknowledgements

One of the authors G. G thanks Council of Scientific & Industrial Research (CSIR), New Delhi for awarding her Senior Research Fellowship. The authors wish to thank The Director, National Institute for Interdisciplinary Science and Technology (NIIST), Thiruvananthapuram, India for his constant encouragement.

References

[1] Jeevanathan P, Mulukutla RS, Phillips M, Chaudhuri M, Erickson LE, Klabunde KJ. Near infrared reflectance properties of metal oxide nanoparticles. Journal of Physical Chemistry C 2007;111:1912–8.
[2] Akbari H, Levinson R, Miller W, Berdahl P. Cool colored roofs to save energy and improve air quality. Santorini: Greece: Proc. International Conf on Passive and Low Energy Cooling for the Built Environment; 2005. p.89.
[3] Bendiganavale AK, Malshe VC. Infrared reflective inorganic pigments. Recent Patents on Chemical Engineering 2008;1:67–79.
[4] Levinson R, Berdahl P, Akbari H, Miller W, Joedicke I, Reilly J, et al. Methods of creating solar-reflective nonwhite surfaces and their application to residential roofing materials. Solar Energy Materials and Solar Cells 2007;91:304–14.
[5] Levinson R, Berdahl P, Akbari H. Solar spectral optical properties of pigments–part II: survey of common colorants. Solar Energy Materials and Solar Cells 2005;89:351–89.
[6] Wake LV. The effect of pigments in formulating solar reflecting and infrared emitting coatings for military applications. Journal of the Oil and Colour Chemists Association 1990;73:78–81.
[7] Kupta KK, Nishkam A, Kasturiya N. Camouflage in the non-visible region. Journal of Industrial Textiles 2001;31:27–42.
[8] Swiler RD, Detrie TJ, Axtell EA. Rare earth transition metal oxide pigments. U.S. Patent 6,582,814;2003.
[9] Modly ZM. High infrared reflecting brown rutile pigment composition, U.S. Patent 5,006,175;1999.
[10] Sliwinski TR, Infrared reflective color pigment. U.S. Patent 6,454,848;2002.
[11] Swiler RD, Axtel EA. Manganese vanadium oxide pigments. U.S. Patent 6,485,557;2002.

[12] Sreeram KJ, Aby CP, Nair BU, Ramasami T. Colored cool colorants based on rare earth metal ions. Solar Energy Materials and Solar Cells 2008;92:1462–7.
[13] Shannon RD. Revised effective ionic radii and systematic studies of interatomic distances in halides and chalcogenides. Acta Crystallographica Section A 1976;32:751–67.
[14] George G, Sandhya Kumari L, Vishnu VS, Ananthakumar S, Reddy MLP. Synthesis and characterization of environmentally benign calcium-doped $Pr_2Mo_2O_9$ pigments: applications in coloring of plastics. Journal of Solid State Chemistry 2008;181:487–92.
[15] Wang XP, Fang QF. Effects of Ca doping on the oxygen ion diffusion and phase transition in oxide ion conductor $La_2Mo_2O_9$. Solid State Ionics 2002;146:185–93.
[16] Chevire F, Munoz CF, Baker CF, Tessier F, Larcher O, Boujday S, et al. UV absorption properties of ceria-modified compositions within the fluorite-type solid solution CeO_2–Y_6WO_{12}. Journal of Solid State Chemistry 2006;179:3184–90.
[17] Chevire F, Clabau F, Larcher O, Orhan E, Tessier F, Marchand R. Tunability of the optical properties in the Y_6(W, Mo)(O, N)$_{12}$ system. Solid State Sciences 2009;11:533–6.
[18] Vishnu VS, George G, Reddy MLP. Effect of molybdenum and praseodymium dopants on the optical properties of $Sm_2Ce_2O_7$: tuning of band gaps to realize various color hues. Dyes and Pigments 2010;85:117–23.
[19] George HC, Ming-Ling L, Li-Dong C, Fu-Qiang H, Daniel EB, Daniel MW, et al. Syntheses, crystal structures, and physical properties of $La_5Cu_6O_4S_7$ and $La_5Cu_{6.33}O_4S_7$. Inorganic Chemistry 2008;47:4368–74.
[20] Sulcova P, Trojan M. Thermal analysis of the Bi_2O_3–Y_2O_3–ZrO_2 pigments. Journal of Thermal Analysis and Calorimetry 2008;93:795–8.
[21] Libbra A, Tarozzi L, Muscio A, Corticelli MA. Spectral response data for development of cool colored tile coverings. Optics and Laser Technology; 2009; doi:10.1016/j.optlastec.2009.07.001.
[22] Smith GB, Gentle A, Swift P, Earp A, Mronga N. Coloured paints based on coated flakes of metal as the pigment, for enhanced solar reflectance and cooler interiors: description and theory. Solar Energy Materials and Solar Cells 2003;79:163–77.
[23] Uemoto KL, Sato NMN, John VM. Estimating thermal performance of cool colored paints. Energy and Buildings 2010;42:17–22.